Analysis and Modeling of Inertial Sensors Using Allan Variance

Naser El-Sheimy, Haiying Hou, and Xiaoji Niu

***Abstract*—It is well known that inertial navigation systems can provide high-accuracy position, velocity, and attitude information over short time periods. However, their accuracy rapidly degrades with time. The requirements for an accurate estimation of navigation information necessitate the modeling of the sensors' error components. Several variance techniques have been devised for stochastic modeling of the error of inertial sensors. They are basically very similar and primarily differ in that various signal processings, by way of weighting functions, window functions, etc., are incorporated into the analysis algorithms in order to achieve a particular desired result for improving the model characterizations. The simplest is the Allan variance. The Allan variance is a method of representing the root means square (RMS) random-drift error as a function of averaging time. It is simple to compute and relatively simple to interpret and understand. The Allan variance method can be used to determine the characteristics of the underlying random processes that give rise to the data noise. This technique can be used to characterize various types of error terms in the inertial-sensor data by performing certain operations on the entire length of data. In this paper, the Allan variance technique will be used in analyzing and modeling the error of the inertial sensors used in different grades of the inertial measurement units. By performing a simple operation on the entire length of data, a characteristic curve is obtained whose inspection provides a systematic characterization of various random errors contained in the inertial-sensor output data. Being a directly measurable quantity, the Allan variance can provide information on the types and magnitude of the various error terms. This paper covers both the theoretical basis for the Allan variance for modeling the inertial sensors' error terms and its implementation in modeling different grades of inertial sensors.**

***Index Terms*—Allan variance, error analysis, gyroscopes, inertial navigation, inertial sensors.**

I. Introduction

An INERTIAL measurement unit (IMU) typically outputs the vehicle's (e.g., aircraft) acceleration and angular rate, which are then integrated to obtain the vehicle's position, velocity, and attitude. The IMU measurements are usually corrupted by different types of error sources, such as sensor noises, scale factor, and bias variations with temperature (nonlinear, difficult to characterize), etc. By integrating the IMU measurements in the navigation algorithm, these errors will be accumulated, leading to a significant drift in the position and velocity outputs. A standalone IMU by itself is seldom useful since the inertial-sensor biases and the fixed-step integration errors will cause the navigation solution to quickly diverge. Inertial systems design and performance prediction depends on the accurate knowledge of the sensors' noise model. The requirements for an accurate estimation of navigation information necessitate the modeling of the sensors' noise components.

The frequency-domain approach for modeling noise by using the power spectral density (PSD) to estimate the transfer functions is straightforward but difficult for nonsystem analysts to understand. Several time-domain methods have been devised for stochastic modeling. The correlation-function approach is the dual of the PSD approach, which is being related as the Fourier transform pair. This is analogous to expressing the frequency response function in terms of the partial fraction expansion. Another correlation method relates the autocovariance to the coefficients of a difference equation, which is expressed as an autoregressive moving-average process. Correlation methods are very model-sensitive and not well suited when dealing with odd power-law processes, higher order processes, or wide dynamic range. They work best with *a priori* knowledge based on a model of few terms [1]. Yet, several time-domain methods have been devised. They are basically very similar and primarily differ in that various signal processings, by way of weighting functions, window functions, etc., are incorporated into the analysis algorithms in order to achieve a particular desired result of improving the model characterizations. The simplest is the Allan variance.

The Allan variance is a time-domain-analysis technique originally developed in the mid-1960s to study the frequency stability of precision oscillators [2]–[7]. Being a directly measurable quantity, it can provide information on the types and magnitude of various noise terms. Because of the close analogies to inertial sensors, this method has been adapted to random-drift characterization of a variety of devices [1], [8]–[12].

Put simply, the Allan variance is a method of representing the root mean square (RMS) random-drift errors as a function of averaging times. It is simple to compute and relatively simple to interpret and understand. The Allan variance method can be used to determine the characteristics of the underlying random processes that give rise to the data noise. In this paper, this technique is used to characterize various types of noise terms in different inertial-sensor data.

Manuscript received June 30, 2005; revised September 3, 2007. This work was supported in part by the Geomatics for Informed Decision Network Centre of Excellence (GEOIDE NCE) and in part by the Natural Sciences and Engineering Research Council (NSERC) of Canada.

N. El-Sheimy is with the Mobile Multisensor Research Group, Department of Geomatics Engineering, University of Calgary, Calgary, AB T2N 1N4, Canada (e-mail: naser@geomatics.ucalgary.ca).

H. Hou is with Schlumberger Drilling & Measurement, Calgary, AB T2C 4R7, Canada (e-mail: haiying407@gmail.com).

X. Niu is with Shanghai SiRF Technology Co., Ltd., Shanghai 200000, China (e-mail: xjniu@sirf.com).

Color versions of one or more of the figures in this paper are available online at http://ieeexplore.ieee.org.

Digital Object Identifier 10.1109/TIM.2007.908635

Although the Allan variance statistic remains useful for revealing broad spectral trends, the Allan variance does not always determine a unique noise spectrum because the mapping from the spectrum to the Allan variance is not one-to-one. This puts a fundamental limitation on what can be learned about a noise process from the examination of its Allan variance.

In the following, the mathematical definition of the Allan variance is given, and the relationship between the Allan variance and the noise PSD is established. Using this relationship, the behavior of the characteristic curve for a number of prominent noise terms can be determined.

II. Methodology

In stochastic modeling, there may be no direct access to an input. A model is hypothesized which, although excited by white noise, has the same output characteristics as the unit under test. The phase information is uniquely determined from the magnitude response. Thus, for a linear time-invariant system, by having a knowledge of the output only, and assuming a white-noise input, it is possible to characterize the unknown model [14]. Such models are not generally unique; thus, certain canonical forms are usually used.

A. Power Spectral Density (PSD)

The PSD is the most commonly used representation of the spectral decomposition of a time series. It is a powerful tool for analyzing or characterizing data and for stochastic modeling. The PSD, or spectrum analysis, is also better suited to analyzing periodic or nonperiodic signals than the other methods [1].

The basic relationship for stationary processes between the two-sided PSD $S(\omega)$ and the covariance $K(\tau)$—the Fourier transform pair—is expressed by

$$S(\omega) = \int_{-\infty}^{\infty} e^{-j\omega\tau} K(\tau) d\tau. \tag{1}$$

The transfer-function form of the stochastic model may be directly estimated from the PSD of the output data (on the assumption of an equivalent white-noise driving function).

For linear systems, the output PSD is the product of the input PSD and the magnitude square of the system transfer function. If state-space methods are used, the PSD matrices of the input and output are related to the system-transfer-function matrix by

$$S_{\text{output}}(\omega) = H(j\omega) S_{\text{input}}(\omega) H^{*\text{T}}(j\omega) \tag{2}$$

where

H	system-transfer-function matrix;
$H^{*\text{T}}$	complex conjugate transpose of H;
S_{output}	output PSD;
S_{input}	input PSD.

Thus, for the special case of the white-noise input, (S_{input} is equal to some constant value, i.e., N_i^2), the output PSD directly gives the system transfer function.

B. Allan Variance

For the Allan variance, the idea is that one or more white-noise sources of strength N_i^2 drive the canonical transfer function(s), resulting in the same statistical and spectral properties as the actual device.

In this paper, Allan's definition and results are related to five basic noise terms and are expressed in a notation appropriate for inertial-sensor data reduction. The five basic noise terms are quantization noise, angle random walk, bias instability, rate random walk, and rate ramp.

Assume that there are N consecutive data points, each having a sample time of t_0. Forming a group of n consecutive data points (with $n < N/2$), each member of the group is a cluster. Associated with each cluster is a time T, which is equal to nt_0. If the instantaneous output rate of the inertial sensor is $\Omega(t)$, the cluster average is defined as

$$\overline{\Omega}_k(T) = \frac{1}{T} \int_{t_K}^{t_k+T} \Omega(t) dt \tag{3}$$

where $\overline{\Omega}_k(t)$ represents the cluster average of the output rate for a cluster which starts from the kth data point and contains the n data points. The definition of the subsequent cluster average is

$$\overline{\Omega}_{\text{next}}(T) = \frac{1}{T} \int_{t_{k+1}}^{t_{k+1}+T} \Omega(t) dt \tag{4}$$

where $t_{k+1} = t_k + T$.

Performing the average operation for each of the two adjacent clusters can form the difference

$$\xi_{k+1,k} = \overline{\Omega}_{\text{next}}(T) - \overline{\Omega}_k(T). \tag{5}$$

For each cluster time T, the ensemble of ξs defined by (5) forms a set of random variables. The quantity of interest is the variance of ξs over all the clusters of the same size that can be formed from the entire data.

Thus, the Allan variance of length T is defined as [8]

$$\sigma^2(T) = \frac{1}{2(N-2n)} \sum_{k=1}^{N-2n} \left[\overline{\Omega}_{\text{next}}(T) - \overline{\Omega}_k(T)\right]^2. \tag{6}$$

Obviously, for any finite number of data points (N), a finite number of clusters of a fixed length (T) can be formed. Hence, (6) represents an estimation of the quantity $\sigma^2(T)$ whose quality of estimate depends on the number of independent clusters of a fixed length that can be formed. The Allan variance can also be defined in terms of the output angle or velocity as

$$\theta(t) = \int^{t} \Omega(t) dt. \tag{7}$$

The lower integration limit is not specified since only the angle or velocity differences are employed in the definitions. The angle or velocity measurements are made at discrete times

given by $t = kt_0, k = 1, 2, 3, \ldots, N$. Accordingly, the notation is simplified by writing $\theta_k = \theta(kt_0)$.

Equations (3) and (4) can then be redefined by

$$\overline{\Omega}_k(T) = \frac{\theta_{k+n} - \theta_k}{T} \tag{8}$$

and

$$\overline{\Omega}_{\text{next}}(T) = \frac{\theta_{k+2n} - \theta_{k+n}}{T}. \tag{9}$$

According to (6), the Allan variance is estimated as follows:

$$\sigma^2(T) = \frac{1}{2T^2(N-2n)} \sum_{k=1}^{N-2n} (\theta_{k+2n} - 2\theta_{k+n} + \theta_k)^2. \tag{10}$$

There is a unique relationship that exists between $\sigma^2(T)$ and the PSD of the intrinsic random processes. This relationship is

$$\sigma^2(T) = 4 \int_0^\infty df \cdot S_\Omega(f) \cdot \frac{\sin^4(\pi f T)}{(\pi f T)^2} \tag{11}$$

where $S_\Omega(f)$ is the PSD of the random process $\Omega(T)$.

In the derivation of (11), it is assumed that the random process $\Omega(T)$ is stationary in time. This assures that the autocorrelation function of $\Omega(T)$ is not dependent on time, and the autocorrelation function is even, which is a necessary condition in the derivation of (11). The detailed derivations can be found in [8] and [17, Sec. 4.2].

Equation (11) states that the Allan variance is proportional to the total power output of the random process when passed through a filter with the transfer function of the form $\sin^4(x)/(x)^2$. This particular transfer function is the result of the method used to create and operate on the clusters.

Equation (11) is the focal point of the Allan-variance method. This equation will be used to calculate the Allan variance from the rate-noise PSD. The PSD of any physically meaningful random process can be substituted in the integral, and an expression for the Allan variance $\sigma^2(T)$ as a function of cluster length can be obtained. Conversely, since $\sigma^2(T)$ is a measurable quantity, a log–log plot of $\sigma(T)$ versus T provides a direct indication of the types of random processes, which exist in the inertial-sensor data. The corresponding Allan variance of a stochastic process may be uniquely derived from its PSD; however, there is no general inversion formula because there is no one-to-one relation [8].

It is evident from (11) and the previous interpretation that the filter bandwidth depends on T. This suggests that different types of random processes can be examined by adjusting the filter bandwidth, namely, by varying T. Thus, the Allan variance provides a means of identifying and quantifying various noise terms that exist in the data. It is normally plotted as the square root of the Allan variance $\sigma(T)$ versus T on a log–log plot. To estimate the amplitude of different noise components, it is convenient to let $n = 2^j, j = 0, 1, 2, \ldots$ [5].

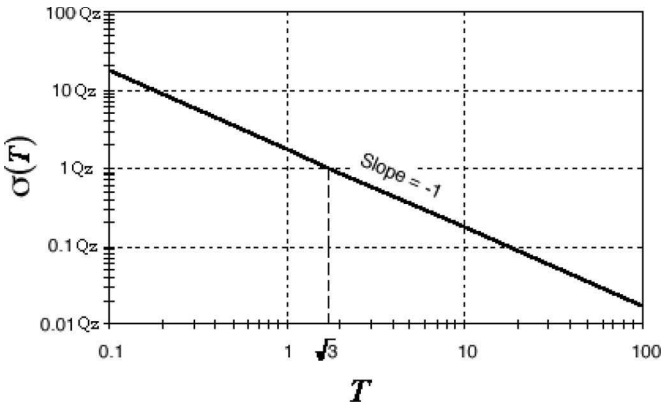

Fig. 1. $\sigma(T)$ plot for quantization noise.

C. Representation of Noise Terms in Allan Variance

The following subsections will show the integral solution for a number of specific noise terms, which are either known to exist in the inertial sensor or are suspected to influence the data. The definition is defined in [1] and [11], and the detailed derivations are given in [8].

1) Quantization Noise: The quantization noise is one of the errors introduced into an analog signal by encoding it in digital form. That noise is caused by the small differences between the actual amplitudes of the points being sampled and the bit resolution of the analog-to-digital converter [13].

For a gyro output, for example, the angle PSD for such a process, as given in [14], is

$$S_\theta(f) = T_\text{s} Q_\text{z}^2 \left(\frac{\sin^2(\pi f T)}{(\pi f T)^2} \right) \approx T_\text{s} Q_\text{z}^2, \qquad f < \frac{1}{2T_\text{s}} \tag{12}$$

where

Q_z quantization-noise coefficient;
T_s sample interval.

The theoretical limit for Q_z is equal to $S/12^{1/2}$, where S is the gyro scaling coefficient for the tests with fixed and uniform sampling times. The gyro rate PSD, on the other hand, is related to the angle PSD through the following relationship:

$$S_\Omega(2\pi f) = (2\pi f)^2 S_\theta(2\pi f) \tag{13}$$

and is

$$S_\Omega(f) = \frac{4Q_\text{z}^2}{T_\text{s}} \sin^2(\pi f T_\text{s}) \approx (2\pi f)^2 T_\text{s} Q_\text{z}^2, \quad f < \frac{1}{2T_\text{s}}. \tag{14}$$

Substituting (14) into (11) and performing the integration yield

$$\sigma^2(T) = \frac{3Q_\text{z}^2}{T^2}. \tag{15}$$

This indicates that the quantization noise is represented by a slope of -1 in a log–log plot of $\sigma(T)$ versus T, as shown in Fig. 1. Here, the unit of time axis in the figure is the relative quantity of the sample time t_0. The magnitude of this noise can be read off as the slope of the line at $T = 3^{1/2}$.

It should be noted that there are other noise terms with different spectral characteristics, such as the flicker angle noise

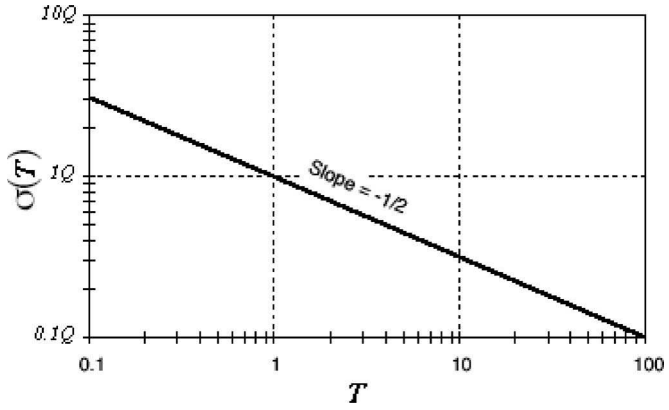

Fig. 2. $\sigma(T)$ plot for angle (velocity) random walk.

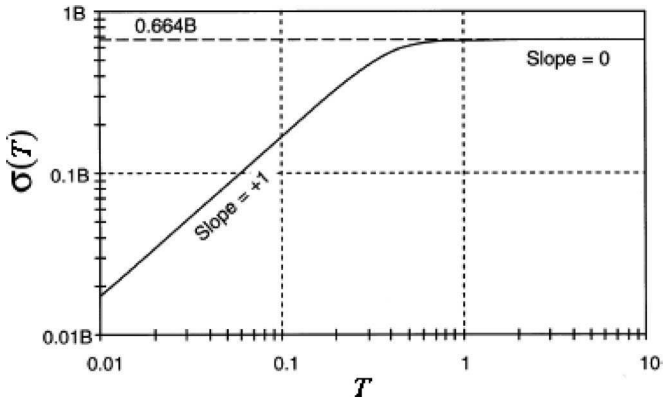

Fig. 3. $\sigma(T)$ plot for bias instability (for $f_0 = 1$) [4] (the value 0.664 in the figure is the result of $\sqrt{2\ln 2/\pi}$).

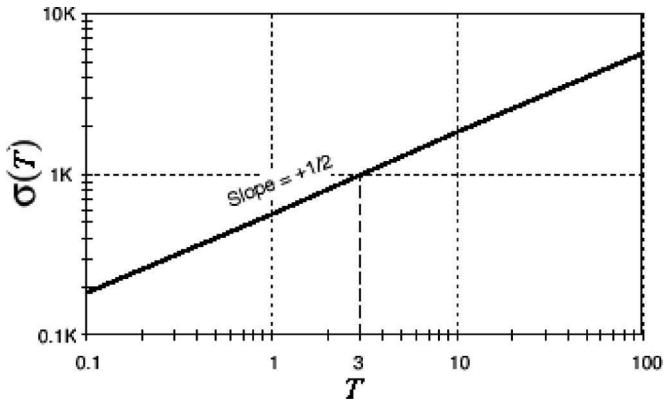

Fig. 4. $\sigma(T)$ plot for rate random walk.

and the white angle noise, which lead to the same Allan-variance T dependence [1].

2) Angle (Velocity) Random Walk: The high-frequency noise terms that have correlation time much shorter than the sample time can contribute to the gyro angle (or accelerometer velocity) random walk. However, most of these sources can be eliminated by design [1]. These noise terms are all characterized by a white-noise spectrum on the gyro (or accelerometer) rate output. The associated rate noise PSD is represented by

$$S_\Omega(f) = Q^2 \tag{16}$$

where Q is the angle (velocity) random-walk coefficient.

Substituting (16) into (11) and performing the integration yield

$$\sigma^2(T) = \frac{Q^2}{T}. \tag{17}$$

As shown in Fig. 2, (17) indicates that a log–log plot of $\sigma(T)$ versus T has a slope of $-1/2$. Furthermore, the numerical value of Q can be directly obtained by reading the slope line at $T = 1$.

3) Bias Instability: The origin of this noise is the electronics or other components that are susceptible to random flickering. Because of its low-frequency nature, it is indicated as the bias fluctuations in the data [15]. The rate PSD associated with this noise is

$$S_\Omega(f) = \begin{cases} \left(\frac{B^2}{2\pi}\right)\frac{1}{f}, & f \le f_0 \\ 0, & f > f_0 \end{cases} \tag{18}$$

where

B bias instability coefficient;

f_0 cutoff frequency.

Substituting (18) into (11) and performing the integration yield

$$\sigma^2(T) = \frac{2B^2}{\pi} \times \left[\ln 2 - \frac{\sin^3 x}{2x^2}(\sin x + 4x\cos x) + C_{\mathrm{i}}(2x) - C_{\mathrm{i}}(4x)\right] \tag{19}$$

where

x $\pi f_0 T$;

C_{i} cosine-integral function.

Fig. 3 shows a log–log plot of (19) that shows that the Allan variance for bias instability reaches a plateau for T much longer than the inverse cutoff frequency. Thus, the flat region of the plot can be examined to estimate the limit of the bias instability.

4) Rate Random Walk: This is a random process of uncertain origin, possibly a limiting case of an exponentially correlated noise with a very long correlation time. The rate PSD associated with this noise is

$$S_\Omega(f) = \left(\frac{K}{2\pi}\right)^2 \frac{1}{f^2} \tag{20}$$

where K is the rate random-walk coefficient.

Substituting (20) into (11) and performing the integration yield

$$\sigma^2(T) = \frac{K^2 T}{3}. \tag{21}$$

This indicates that the rate random walk is represented by a slope of $+1/2$ on a log–log plot of $\sigma(T)$ versus T, as shown in Fig. 4. The magnitude of this noise, K, can be read off as the slope line at $T = 3$.

5) Drift Rate Ramp: The error terms considered so far are of random character. It is, however, useful to determine the

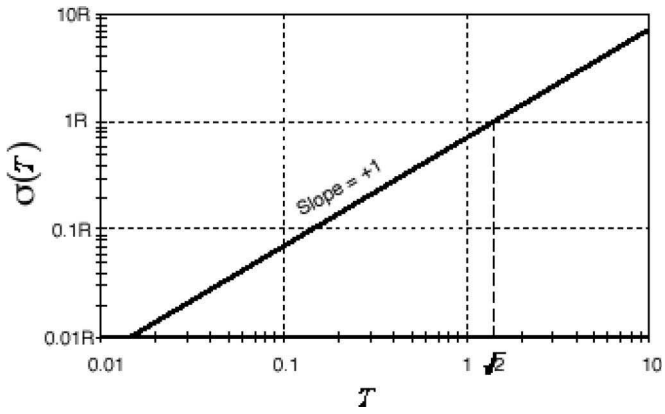

Fig. 5. $\sigma(T)$ plot for drift rate ramp.

behavior of $\sigma(T)$ under systematic (deterministic) errors. One such error is the drift rate ramp defined as

$$\Omega = Rt \tag{22}$$

where R is the drift-rate-ramp coefficient.

By forming and operating on the clusters of data containing an input given by (22), we obtain

$$\sigma^2(T) = \frac{R^2T^2}{2}. \tag{23}$$

This indicates that the drift-rate-ramp noise has a slope of $+1$ in the log–log plot of $\sigma(T)$ versus T, as shown in Fig. 5. The amplitude of drift rate ramp R can be obtained from the slope line at $T = 2^{1/2}$.

The rate PSD associated with this noise is

$$S_\Omega(f) = \frac{R^2}{(2\pi f)^3}. \tag{24}$$

It should be noted that there might be a flicker acceleration noise with $1/f^3$ PSD that leads to the same Allan-variance T dependence [1].

D. Estimation Quality of Allan Variance

With real data, gradual transitions would exist between the different Allan standard-deviation slopes. A certain amount of noise or hash would exist in the plot curve due to the uncertainty of the measured Allan variance [11]. In practice, the estimation of the Allan variance is based on a finite number of independent clusters that can be formed from any finite length of data. The confidence of the estimation improves as the number of independent clusters is increased.

Defining the parameter δ as the percentage error in estimating the Allan standard deviation of the cluster due to the finiteness of the number of clusters

$$\delta = \frac{\sigma(T, M) - \sigma(T)}{\sigma(T)} \tag{25}$$

where $\sigma(T, M)$ denotes the estimate of the Allan standard deviation obtained from M independent clusters; $\sigma(T, M)$ approaches its theoretical value $\sigma(T)$ in the limit of M approaching infinity. A lengthy but straightforward [16] calculation shows that the percentage error is equal to

$$\sigma(\delta) = \frac{1}{\sqrt{2\left(\frac{N}{n} - 1\right)}} \tag{26}$$

where N is the total number of data points in the entire run, and n is the number of data points contained in the cluster.

Equation (26) shows that the estimation errors in the region of short cluster length T are small as the number of independent clusters in these regions is large (small). On the contrary, the estimation errors in the region of long cluster length T are large as the number of independent clusters in these regions is small. For example, if there are 2000 data points and the cluster sizes of 500 points are used, the percentage error in estimating $\sigma(T)$ is approximately 40%. On the other hand, for the cluster containing only ten points, the percentage error is about 5%.

III. Test Environment

Three different-grade IMUs were involved in evaluating the use of Allan variance in modeling inertial-sensor noise. The IMUs include the Honeywell CIMU navigation-grade IMU, the Honeywell HG1700 tactical-grade IMU, and the Systron Donner MotionPak II-3g MEMS-grade IMU. The test was held at room temperature for seven days at the Inertial Laboratory, Mobile Multi-Sensor System Group, Department of Geomatics Engineering, University of Calgary. Some 4-h static data were collected in each test, and the most stable 2-h data were extracted for analysis. The test layout and the equipment used in this test are shown in Figs. 6 and 7. The following sections detail the characteristics of the tested IMUs and the data acquisition systems.

A. CIMU—Navigation-Grade IMU

The Commercial Inertial Measurement System (CIMU) [Fig. 6(b)] is a relevant small (i.e., a cube of 13.4 cm in height with 19.3-cm length and 16.9-cm width) navigation-grade IMU manufactured by Honeywell International, Inc. The gyro in the run bias is about $0.0022^\circ/\text{h}$, and the random walk is about $0.0022^\circ/\text{h}^{1/2}$. The accelerometer in the run bias is about 25 μg, and the noise is about 0.00076 m/s/h$^{1/2}$ (0.0025 FPS/h$^{1/2}$).

B. HG1700—Tactical-Grade IMU

The Honeywell HG1700 [Fig. 6(b)] is a cylinder that is 7.6 cm in height and 9.4 cm in diameter and is a light-weight and low-cost tactical-grade IMU that utilizes three GG1308 miniature ring laser gyros along with three Honeywell RBA-500 resonant beam digital accelerometers to measure the angular rate and linear acceleration. This IMU has a gyro bias repeatability of better than $3^\circ/\text{h}$, a gyro scale-factor accuracy of better than 150 ppm, and a gyro random-walk PSD level of less than $0.15^\circ/\text{h}^{1/2}$. The accelerometer residual bias is less than 1000 μg, the scale-factor stability is 300 ppm, and the linearity is 500 ppm.

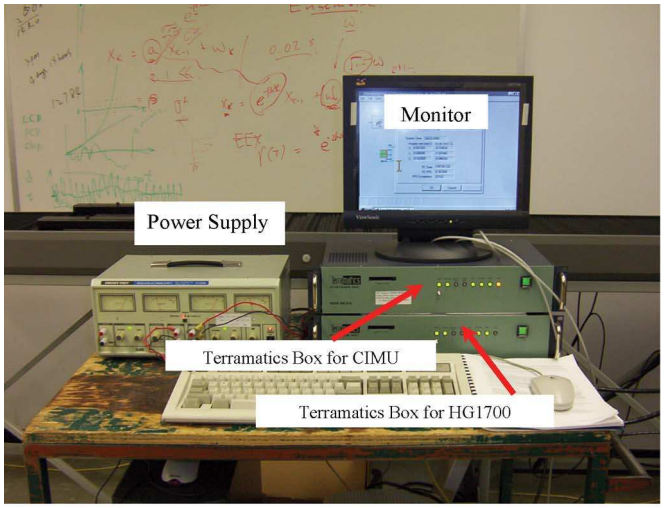

(a)

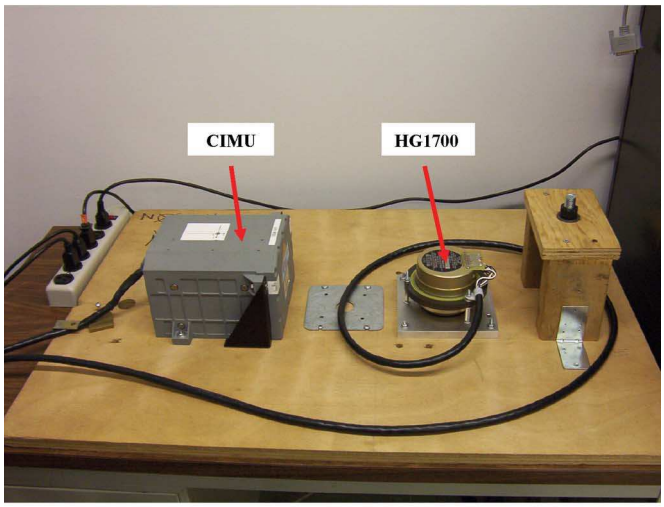

(b)

Fig. 6. Test setup to collect the IMU data for the Allan-variance analysis. (a) Data loggings. (b) IMUs.

C. MotionPak II—Consumer-Grade MEMS-Based IMU

The MotionPak is a solid-state six degree-of-freedom IMU used for measuring linear accelerations and angular rates in instrumentation and control applications. It uses three orthogonally mounted solid-state micromachined quartz angular-rate sensors and three linear servo accelerometers. The maximum bias error is $\pm 5^{\circ}/\mathrm{s}$ for gyro and ± 200 mg for accelerometers. The bandwidth, with flat ± 3 dB, is larger than 30 Hz for gyro and 250 Hz for accelerometer.

For this unit, the data were collected using a multifunction 16-b data-acquisition card from the National Instruments, the DAQCard-6036E, which is controlled by a script based on the National Instrument LabVIEW 7.0.

IV. Test Result

A. CIMU Allan-Variance Analysis

The 2-h static data from the CIMU were collected at room temperature. By applying the Allan-variance method to the whole data set, a log–log plot of the Allan standard deviation versus the cluster time is shown in Fig. 8 for the gyro data and Fig. 9 for the accelerometer data. As shown in these figures, the quality of the calculated Allan variance varied from the short cluster (left side, error of 0.06%) to the long one (right side, error of 40%). Fig. 8 clearly shows that, for the CIMU gyro data, the quantization noise is the dominant noise for the short cluster times. For the X-axis gyro curve, for example, a straight line with a slope of -1 fitted to the beginning of the curve meets the vertical line of $T = 3^{1/2}$ hour line (see Fig. 1 for details) at a value of $2.70 * 10^{-4}$ deg, which is equivalent to 0.973 arcsec. Since the estimation of quantization noise is based on very short cluster times, the number of independent cluster is very large, and the quality of estimation is very good. In fact, even for a cluster time as long as $T = 100$ s, the percentage error is 7.6%. Thus, the quantization coefficient for CIMU X-axis gyro is estimated as

$$Q_{\mathrm{z}} = (0.973 \pm 0.074)\ \mathrm{arcsec}. \tag{27}$$

Table I lists the estimated quantization-noise coefficients for the seven-day tests for all the three-axis gyros. The table clearly indicates that the standard deviation of the seven-day tests is smaller than the estimation percentage error (compared with the results in Table II). This simply means that the CIMU sensor random processes have very good repeatability. As a result, each of these individual tests of the CIMU gyros can be used as a representative for the gyro performance.

Fig. 8 also shows that the CIMU gyros exhibit an angle random walk for long cluster times. For example, for the X-axis curve, a straight line with a slope of $-1/2$ fits to the long cluster-time part of the plot and meets the vertical line at $T = 1$ hour line (see Fig. 2) at a value of 0.0015. The inspection of the curve shows that the estimation percentage error in this region can reach 33%. Thus, the angle random-walk coefficient for the CIMU X-axis gyro is estimated as

$$Q = (0.0015 \pm 0.0005)\ \mathrm{deg}/\sqrt{\mathrm{h}}. \tag{28}$$

The unit of the angular random walk $\mathrm{deg}/\sqrt{\mathrm{h}}$ is the convention unit in the inertial society. Its conversion to the standard metric unit is as follows:

$$\begin{aligned} 1\mathrm{deg}/\sqrt{\mathrm{h}} &= 1 * \mathrm{pi}/180\ \mathrm{rad}/\sqrt{(3600\ \mathrm{s})} \\ &= 2.9 * 10^{-4}\ \mathrm{rad}/\sqrt{\mathrm{s}} = 2.9 * 10^{-4}\ \mathrm{rad/s}/\sqrt{\mathrm{Hz}}. \end{aligned}$$

The corresponding unit for the velocity random walk of accelerometers is $\mathrm{m/s}/\sqrt{\mathrm{h}}$, which will be later used in this paper. Similarly, the conversion to the metric unit is

$$\begin{aligned} 1\ \mathrm{m/s}/\sqrt{\mathrm{h}} &= 1 * \mathrm{m/s}/\sqrt{(3600\ \mathrm{s})} \\ &= 0.0167\ \mathrm{m/s}/\sqrt{\mathrm{s}} = 0.0167\ \mathrm{m/s^2}/\sqrt{\mathrm{Hz}}. \end{aligned}$$

For the CIMU accelerometer data, the Allan-variance results that are shown in Fig. 9 clearly show that the quantization noise is the prominent error term in the short cluster times, whereas it is the drift rate-ramp term in the long cluster times.

For example, for the X-axis plot, a straight line with a slope of $+1$ fits the long cluster-time part of the plot and meets the

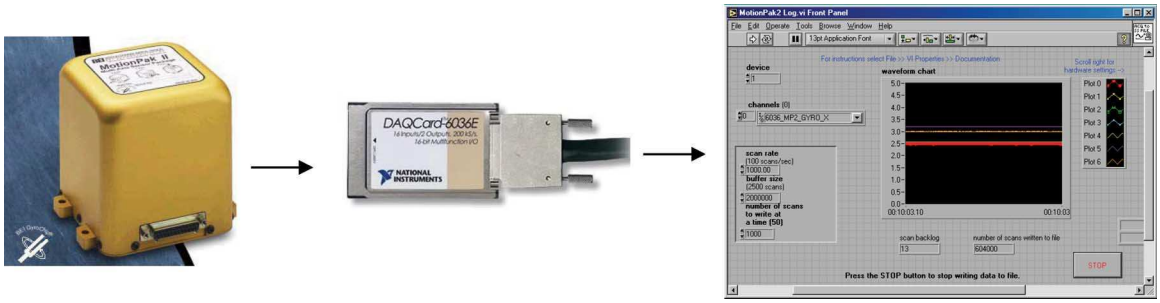

Fig. 7. Data logging system of MEMS IMU (MotionPak II).

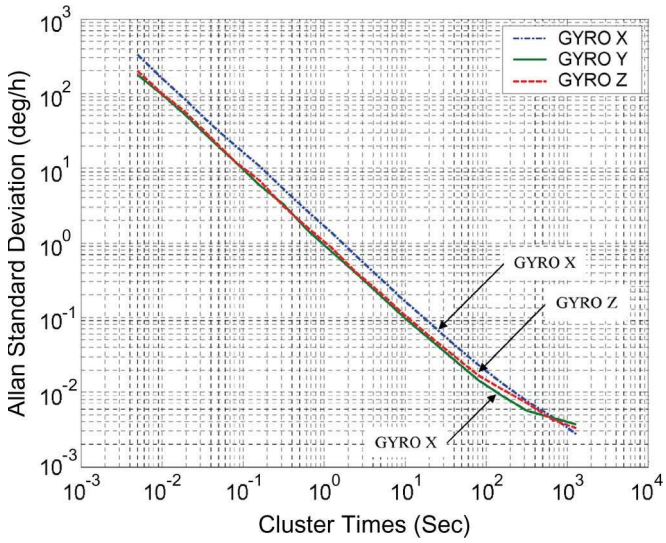

Fig. 8. CIMU gyro Allan-variance results.

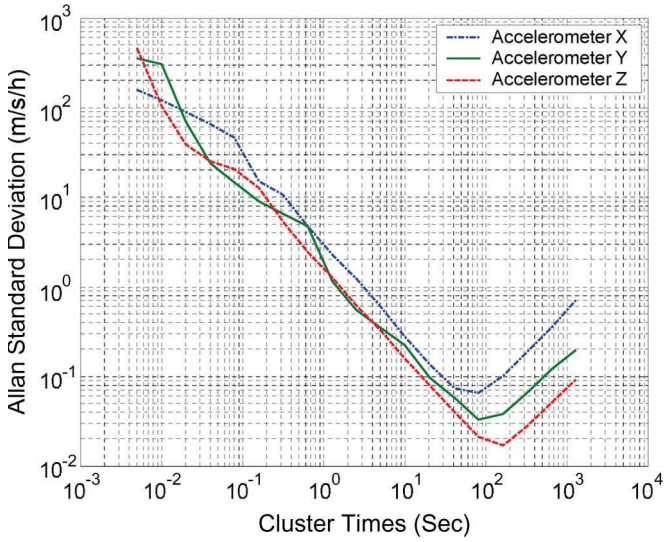

Fig. 9. CIMU accelerometer Allan-variance results.

vertical line at $T = 2^{1/2}$ hour line (see Fig. 5) at a value of 2.64. The inspection of the curve shows that the estimation percentage error in this region can reach 33%. Thus, the drift rate-ramp coefficient for the CIMU X-axis accelerometer is estimated as

$$R = (2.64 \pm 0.88)\ \text{m/s/h}^2. \tag{29}$$

TABLE I
CIMU GYRO QUANTIZATION-NOISE ESTIMATION RESULTS

Test #	Gyro X (arcsec)	Gyro Y (arcsec)	Gyro Z (arcsec)
1	0.973	0.517	0.577
2	0.960	0.536	0.602
3	0.919	0.506	0.575
4	0.947	0.498	0.569
5	0.958	0.499	0.559
6	0.959	0.507	0.562
7	0.945	0.507	0.579
STD	0.017	0.013	0.014

TABLE II
IDENTIFIED ERROR COEFFICIENTS FOR CIMU

	Quantization noise (arcsec)	Angular Random Walk (deg/√h)
Gyro X	0.973±0.074	0.0015±0.0005
Gyro Y	0.517±0.020	0.0019±0.0006
Gyro Z	0.577±0.016	0.0018±0.0006
	Quantization noise (m/s/h)	Acceleration drift ramp (m/s/h^2)
Accl X	1.680±0.128	2.64±0.88
Accl Y	1.298±0.099	0.89±0.30
Accl Z	0.879±0.067	0.39±0.13

Table II lists the identified error coefficients for all of the CIMU gyro and accelerometer sensors.

B. HG1700 Allan-Variance Analysis

Th 2-h static data from the HG1700 was collected at room temperature. By applying the Allan-variance method to the whole data set, a log–log plot of the Allan standard deviation versus the cluster time is shown in Fig. 10 for the gyro data. The results clearly indicate that the quantization noise is the dominant error for the short cluster times, whereas the angle random walk is the dominant error for the long cluster times.

Table III summarizes the estimated quantization error coefficients for the seven-day tests for the three gyros. The results indicate that the standard deviation of the seven-day tests is close to the estimation percentage error (as shown in Table IV), which means that the HG1700 sensor random processes have relevantly good repeatability. This means that each individual test result of the HG1700 can be used as a representative for the gyro performance used in the system.

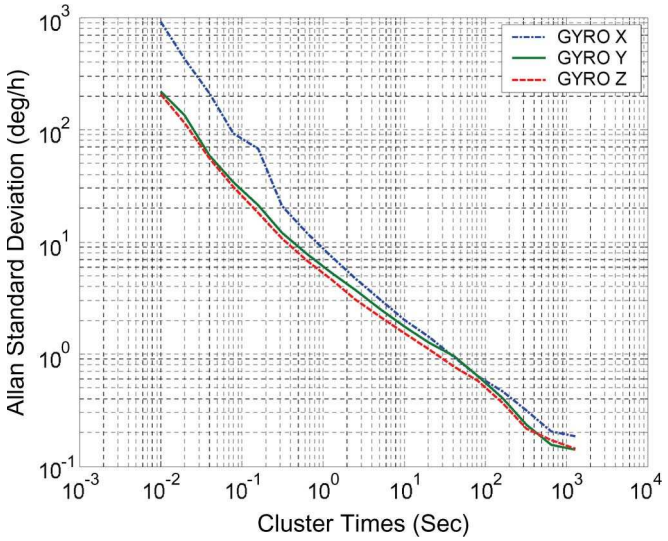

Fig. 10. HG1700 gyro Allan-variance results.

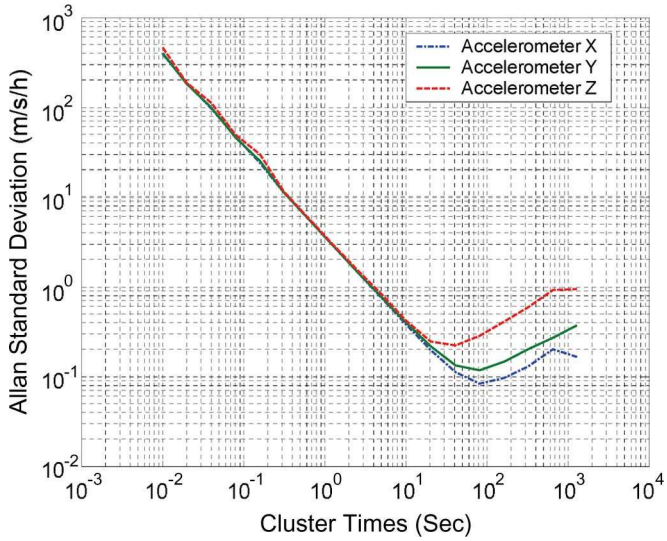

Fig. 11. HG1700 accelerometer Allan-variance results.

TABLE III
HG1700 GYRO QUANTIZATION-NOISE ESTIMATION RESULTS

Test #	Gyro X (arcsec)	Gyro Y (arcsec)	Gyro Z (arcsec)
1	5.115	1.274	1.232
2	5.112	1.284	1.203
3	5.111	1.280	1.223
4	5.124	1.307	1.226
5	5.031	1.286	1.219
6	5.105	1.305	1.207
7	5.049	1.295	1.223
STD	0.037	0.012	0.010

TABLE IV
IDENTIFIED ERROR COEFFICIENTS FOR HG1700

	Quantization noise (arcsec)	Angular Random Walk (deg/√h)
Gyro X	5.1154±0.068	0.094±0.031
Gyro Y	1.2742±0.0032	0.088±0.030
Gyro Z	1.2316±0.0028	0.075±0.026
	Quantization noise (m/s/h)	Acceleration random walk ($m/s/h^{3/2}$)
Accl X	2.119±0.067	0.76±0.25
Accl Y	2.199±0.118	1.16±0.39
Accl Z	2.185±0.058	3.35±1.12

Fig. 11 shows the Allan-variance results for the HG1700 accelerometer data. It is seen that the quantization noise is the dominant error term in the short cluster times, whereas the rate random walk is the dominant error in the long cluster times. Table IV summarizes the identified error coefficients for all the sensors in the HG1700 unit. Please note that the 2-h static data are not enough for the complete modeling of the navigation-grade IMU (CIMU) and the tactical-grade IMU (HG1700). The long-term errors, like bias instability, require much longer static data to be used (about 100 h), which was not possible within the test setup used in this paper.

C. MotionPak II Allan-Variance Analysis

Since the data sampling rate will affect the Allan-variance result and considering the fact that the MotionPak II provides an analog data, different sampling rate data sets were collected for the system through the A/D card. Using the A/D card, the 10-min data sets at different sampling rates (10, 50, 100, 500, 1000, and 2000 Hz) were collected. Fig. 12 shows the results of the Allan variance of these data sets.

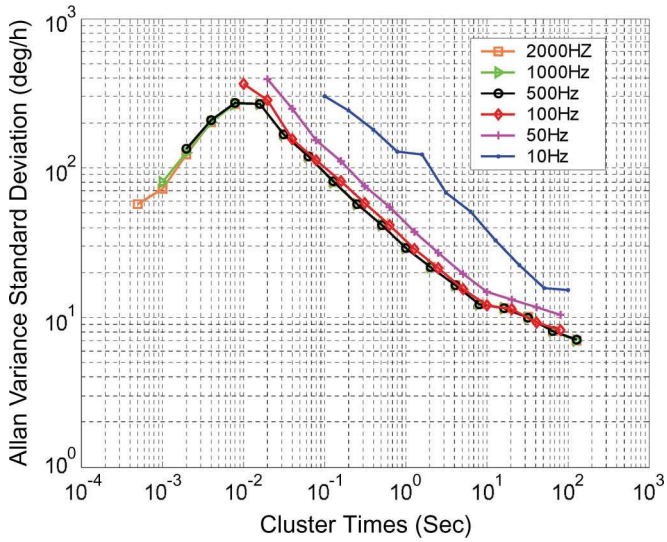

Fig. 12. MotionPak II gyro (X-axis) Allan-variance results with different sampling rates.

Fig. 12 clearly shows that the Allan-variance curves of the MotionPak II are almost the same, as long as the sampling rate is higher than 100 Hz. However, when the sampling rate is further reduced to 50 and 10 Hz, the Allan curves shifted, which is because the sampling rate is low enough to satisfy the Nyquist theorem. From the data sheet of MotionPak II, the bandwidth of gyros is larger than 30 Hz. Therefore, the sampling rate should reach three-to-five times the sensor bandwidth to meet the requirement for reliable sensor-performance analysis. Here, we chose the sample rate for the MotionPak II gyro at 100 Hz. The attenuation in the high-frequency part (i.e., $T < 0.01$ s) is the embodiment of the sensors' bandwidth (30 Hz, as previously mentioned). For short cluster-time span ($T < 10$ s),

TABLE V
IDENTIFIED ERROR COEFFICIENTS FOR MOTIONPAK II

Sensor	Angular Random Walk (deg/√h)	Bias Instability (deg/h)
Gyro X	0.512±0.007	13.6±1.4
Gyro Y	0.486±0.007	11.7±1.2
Gyro Z	0.489±0.007	16.8±1.7
	Velocity Random Walk (m/s/√h)	Bias Instability (m/s/h)
Accl X	0.0166±0.00003	4.36±0.04 (m/s/h)
Accl Y	0.0159±0.00003	4.09±0.08 (m/s/h)
Accl Z	0.0161±0.00003	4.36±0.08 (m/s/h)

the angular random walk is the dominant error source. Starting from the cluster time longer than 10 s, the curve tends to be level. A valley bottom in the Allan-variance plot for the 2-h static data set corresponds to the bias instability error. The Allan-variance estimation results are shown in Table V. The results clearly indicate that, for the MotionPak II sensors, the random walk is the dominant error in the short cluster time, whereas the bias instability term is the dominant error in the long cluster time.

V. CONCLUSION

The Allan-variance method presented in this paper allows a systematic characterization of the various random errors contained in the output data of the inertial sensor. By performing a simple operation on the entire length of data, a characteristic curve is obtained whose inspection facilitates the determination of the different types and magnitude of error terms existing in the inertial sensors.

The seven-day static data from the CIMU, HG1700, and MotionPak II-3g were investigated. Most of the results from the Allan-variance analysis are close to the manufacturers' claim, which prove that the method performed in this paper is valid. The results of the data analysis indicate the following.

1) For the CIMU and the HG1700, the quantization noise is the dominant error term in the short cluster times for both the gyros and accelerometers and the angular random walk is the dominant error in the long cluster times (up to 1800 s) for the gyros, whereas the acceleration drifts (include the random walk and ramp) are the dominant errors in the long cluster times (up to 1800 s) for the accelerometers.
2) The results of the MotionPak II sensors clearly indicate that the random walk is the dominant error term in the short cluster time, whereas the bias instability terms are the dominant error in the long cluster time.
3) When collecting the analog signals through an A/D card for the Allan-variance analysis, the Nyquist theorem should be considered. The recommended sampling rate should be three to five times the sensor bandwidth to guarantee the validity of the Allan-variance analysis to the sensor performance.

This paper clearly shows that the Allan variance is a powerful technique to investigate the sensor error behaviors on different timescales. The Allan-variance analysis is an effective method for error modeling and parameter estimation. Its application is not necessarily to be limited to the oscillator and inertial sensors but can be extended to other types of sensors.

REFERENCES

[1] *IEEE Standard Specification Format Guide and Test Procedure for Single-Axis Interferometric Fiber Optic Gyros,* IEEE Std. 952-1997, 1998.
[2] D. W. Allan, "Statistics of atomic frequency standards," *Proc. IEEE*, vol. 54, no. 2, pp. 221–230, Feb. 1966.
[3] P. Lesage and C. Audoin, "Characterization of frequency stability: Uncertainty due to the finite number of measurements," *IEEE Trans. Instrum. Meas.*, vol. IM-22, no. 2, pp. 157–161, Jun. 1973.
[4] D. W. Allan and J. A. Barnes, "A modified "Allan Variance" with increased oscillator characterization ability," in *Proc. 35th Annu. Freq. Control Symp.*, May 1981, pp. 470–475.
[5] D. W. Allan, "Time and frequency (time-domain) characterization, estimation, and prediction of precision clocks and oscillators," *IEEE Trans. Ultrason., Ferroelectr., Freq. Control*, vol. UFFC-34, no. 6, pp. 647–654, Nov. 1987.
[6] J. W. Chaffee, "Relating the Allan variance to the diffusion coefficients of a linear stochastic differential equation model for precision oscillators," *IEEE Trans. Ultrason., Ferroelectr., Freq. Control*, vol. UFFC-34, no. 6, pp. 655–658, Nov. 1987.
[7] B. L. Conroy and D. Le, "Measurement of Allan variance and phase noise at fractions of a millihertz," *Rev. Sci. Instrum.*, vol. 61, no. 6, pp. 1720–1723, Jun. 1990.
[8] M. M. Tehrani, "Ring laser gyro data analysis with cluster sampling technique," *Proc. SPIE*, vol. 412, pp. 207–220, 1983.
[9] A. D. King, "Characterization of gyro in-run drift," in *Proc. Symp. Gyro Technol.*, Oct. 1984, pp. 10.0–10.56.
[10] S. H. Stovall, "Analysis of ring laser gyro noise measurement techniques," NWC, China Lake, CA, 1987. Tech. Rep.
[11] *IEEE Standard Specification Format Guide and Test Procedure for Linear, Single-Axis, Non-Gyroscopic Accelerometers,* IEEE Std. 1293-1998, 1999.
[12] H. Hou and N. El-Sheimy, "Inertial sensors errors modeling using Allan variance," in *Proc. ION GPS/GNSS*, Portland, OR, Sep. 9–12, 2003, pp. 2860–2867. Best Presentation Winning Paper, U.S. Inst. Navigation.
[13] Wikipedia, "Quantization error," retrieved on Nov. 8, 2007. [Online]. Available: en.wikipedia.org/wiki/Quantization_error
[14] A. Papoulis, *Probability, Random Variables, and Stochastic Process*, 3rd ed. New York: McGraw-Hill, 1991.
[15] M. S. Keshner, "1/f Noise," *Proc. IEEE*, vol. 70, no. 3, pp. 212–218, Mar. 1982.
[16] J. A. Barnes *et al.*, "Characterization of frequency stability," *IEEE Trans. Instrum. Meas.*, vol. IM-20, no. 2, pp. 105–120, May 1971.
[17] H. Hou, "Modeling inertial sensors errors using Allan variance," M.S. thesis, MMSS Res. Group, Dept. Geomatics Eng., Univ. Calgary, Calgary, AB, Canada, UCGE Rep. 20201, Sep. 2004. [Online]. Available: http://www.geomatics.ucalgary.ca/Papers/Thesis/NES/04.20201.HaiyingHou.pdf

Naser El-Sheimy received the B.Sc. and M.Sc. degrees from Ain Shams University, Cairo, Egypt, in 1994 and 1990, respectively, and the Ph.D. degree from the University of Calgary, Calgary, AB, Canada, in 1996.

He is currently a Professor, the Team Leader of the Mobile Multisensor Research Group, and the Head of the Department of Geomatics Engineering, University of Calgary. He is also the Canada Research Chair of Mobile Multisensors Geomatics Systems. His research interests include the integration of GPS/inertial navigation systems/imaging sensors for mapping and geographic information systems applications, with special emphasis on the use of multisensors in mobile mapping systems.

Dr. El-Sheimy is the Chair of the Working Group on Integrated Mobile Mapping Systems, International Society for Photogrammetry and Remote Sensing, the Vice Chair of the Special Study Group for Mobile Multisensor Systems, International Association of Geodesy, and the Chair of the Working Group C5.3 on Integrated Positioning, Navigation, and Mapping Systems, International Federation of Surveyors.

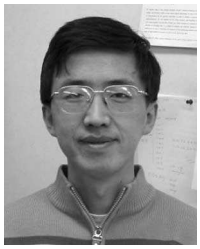

Haiying Hou received the B.Eng. degree in industry automation from the Harbin Engineering University, Harbin, China, in 1996 and the M.S. degree in geomatics engineering from the University of Calgary, Calgary, AB, Canada, in 2004.

He is currently an Electrical Technologist with Schlumberger Drilling & Measurement, Calgary. In 1996, he was with the Harbin Engineering University as an Electrical Engineer, designing interface boards for integrated navigation consoles for five years. He is currently an Assistant Engineer with Schlumberger, Ltd., Calgary. His research interests include positioning, navigation, and attitude determination using integrated navigation systems.

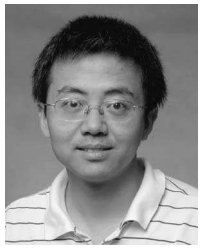

Xiaoji Niu received the B.Eng. degree (with honors) in mechanical and electrical engineering and the Ph.D. degree from Tsinghua University, Beijing, China, in 1997 and 2002, respectively.

He is currently a Senior Scientist with SiRF Technology, Inc., Shanghai SiRF Technology Co., Ltd., Shanghai, China. Since 2003, he has been a Postdoctoral Fellow with the Mobile Multisensor Systems Research Group, Department of Geomatics Engineering, University of Calgary, Calgary, AB, Canada. His research interests include low-cost GPS/inertial navigation technology for vehicles and pedestrians.